Eur. Phys. J. D **19**, 103–109 (2002)
DOI: 10.1140/epjd/e20020061

THE EUROPEAN PHYSICAL JOURNAL D
EDP Sciences

Production of a Bose Einstein condensate of metastable helium atoms

F. Pereira Dos Santos[1,a], J. Léonard[1], Junmin Wang[1,b], C.J. Barrelet[1], F. Perales[2], E. Rasel[3], C.S. Unnikrishnan[4], M. Leduc[1], and C. Cohen-Tannoudji[1]

[1] Collège de France and Laboratoire Kastler Brossel[c], Département de Physique de l'École Normale Supérieure, 24 rue Lhomond, 75231 Paris Cedex 05, France
[2] Laboratoire de Physique des Lasers[d], Université Paris-Nord, avenue J.B. Clément, 93430 Villetaneuse, France
[3] Universität Hannover, Welfengarten 1, 30167 Hannover, Germany
[4] TIFR, Homi Bhabha Road, Mumbai 400005, India

Received 15 October 2001

Abstract. We recently observed a Bose-Einstein condensate in a dilute gas of ^{4}He in the 2^3S_1 metastable state. In this article, we describe the successive experimental steps which led to the Bose-Einstein transition at 4.7 μK: loading of a large number of atoms in a MOT, efficient transfer into a magnetic Ioffé-Pritchard trap, and optimization of the evaporative cooling ramp. Quantitative measurements are also given for the rates of elastic and inelastic collisions, both above and below the transition.

PACS. 32.80.Pj Optical cooling of atoms; trapping – 03.75.Fi Phase coherent atomic ensembles; quantum condensation phenomena – 05.30.Jp Boson systems

1 Introduction

Recently two groups in France reported the first observation of Bose Einstein condensation (BEC) of helium 4 atoms in the 2^3S_1 metastable state [1,2], following the condensation of ^{87}Rb, ^{23}Na, and ^{7}Li in 1995 [3–5] and of atomic hydrogen in 1998 [6]. The method to reach BEC with metastable helium atoms uses similar routes as for alkali atoms, namely laser cooling and trapping followed by a final step of evaporative cooling.

However the case of the metastable helium BEC is different from all the other atomic condensates. It carries a large internal energy (19.8 eV per atom), which can be exploited in several ways. For instance, each atom can be detected with a large efficiency, almost one by one [1]. Also, the collision with most of the atoms and molecules results in ionization (Penning ionization).

The aim of the present article is to precisely describe the experimental procedure used to reach metastable helium BEC by our group at ENS. We describe briefly the preparation of the cold cloud in an optimized magneto-optical trap (MOT) and give details on the optical detection scheme. The subsequent loading into a tight magnetostatic trap as well as the evaporative cooling phase are discussed. Relevant collisional parameters and results from phase transition measurements are given and discussed.

2 MOT

Despite the fact that producing a MOT has become routine in many laboratories, some care has to be taken when one has to produce a MOT intended as the first step towards BEC. It is necessary to trap a sample containing a large number of atoms, with a lifetime as long as possible. In this respect, metastable helium is more delicate in comparison with alkalis. First, one has to start by exciting the ground state helium beam (by electron bombardment through a high voltage discharge), and this process has a low efficiency. Second, metastable helium atoms have very large inelastic collision rates in a MOT, due to Penning collisions enhanced by light, which severely limit the atomic density.

The loading of the MOT is explained in detail in reference [7]. The cold gas of helium atoms is first trapped into a MOT at the center of a small quartz cell ($4 \times 4 \times 5$ cm), evacuated by a turbo molecular pump. The ultra high vacuum without the atomic beam running is on the order of 10^{-11} torr, and increases to about 5×10^{-11} when the atomic beam is on. A description of the infrared laser we use to manipulate the metastable atoms can be

[a] e-mail: franck.pereira-dos-santos@lkb.ens.fr
[b] *Permanent address*: Institute of Opto-Electronics, Shanxi University, Taiyuan, Shanxi 030006, P.R. China.
[c] Unité de Recherche de l'École normale supérieure et de l'Université Pierre et Marie Curie, associée au CNRS (UMR 8552).
[d] UMR 7538 du CNRS

found in [7]. It operates at 1083 nm on the $2^3S_1 \rightarrow 2^3P_2$ transition. It uses a laser diode oscillator followed by an Yb doped fiber amplifier, which results in a robust user friendly laser system requiring neither maintenance nor frequent readjustment.

The coils Q1 and Q2 of the MOT are the same as those used in the magnetostatic trap described in Section 4.1 (see Fig. 2): they have 144 turns each, the current is 6.5 A and the field gradient they produce along the axis y of symmetry is 55 gauss/cm.

For the MOT, the detuning of the laser beams δ is large, -45 MHz (namely 28Γ, where Γ is the inverse lifetime of the 2^3P_2 state). Such a large detuning is chosen in order to minimize the population in the 2^3P_2 state, which reduces the rate of light assisted Penning ionizing collisions. To compensate for the large detuning, the intensity of the beams is also large, 8 mW/cm^2 per beam. The size of these beams is typically 2 cm in diameter. Despite this, the half-life of the MOT is only 100 ms, because of the Penning collisions, which is much lower than the typical decay time of any alkali MOT. The loading time of the MOT from the Zeeman slowed beam is thus short: the steady state of the MOT is reached in 1 s. The total number of trapped atoms is measured, according to the procedure described in [8], to be 10^9 atoms, with a temperature of about 1 mK (which corresponds to a mean velocity of 1 m/s), and rms radii of 2 mm in the weakest axis of the quadrupole.

3 Optical detection of the cold cloud

The same optical detection scheme of the cold cloud is used through all the temperature range from the MOT down to the condensate. It is represented in Figure 1. The source is a DBR laser diode (SDL-6702-H1), operating at 1083 nm. It propagates through an optical fiber, is then expanded to a diameter of about 1 cm and finally sent through the quartz cell (which is not antireflection coated). Its polarization is circular and it operates at resonance with the atomic frequency. We image the shadow of the atomic cloud on a CCD camera using achromat doublet lenses.

The camera (model Hamamatsu C4880) has a low quantum efficiency at 1.08 μm, which we measured to be 1.5%. In order to obtain a sufficient signal to noise ratio on the pictures, it is required to operate at not too low an intensity (typically $I/I_{\rm sat} = 0.2$), with large exposure times (typically 100 μs) and a moderate magnification. The magnification of the imaging system is chosen to be 1, which we use to observe the cold gas at all stages of the experiment, from the gas in the large size MOT to the small condensed cloud. The resolution is thus limited to 24 μm by the pixel size of the camera. One uses a standing wave in order to avoid as much as possible any pushing effect due to the radiation pressure occurring if a travelling wave were used. But in this configuration, the impact on the absorption of the residual kinetic effects is difficult to determine.

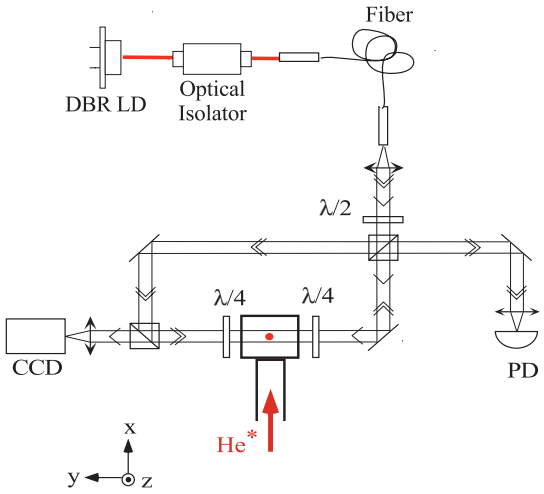

Fig. 1. Detection setup. DBR LD is a Distributed Bragg Reflector Laser Diode, PD a photodiode and CCD a CCD camera.

From the absorption images taken by the camera we extract the size and the temperature of the cloud. Deducing the absolute number of atoms with a good precision from these pictures turned out to be a difficult task, as already discussed in [2].

To measure the total number of atoms, we illuminate the cloud with the probe beam at resonance, but in a travelling wave configuration here. The detection set-up sketched in Figure 1 allows one to switch from a standing to a travelling wave, by simply rotating a $\lambda/2$ plate. We measure the power absorbed in the probe beam on the photodiode PD (see Fig. 1). When the intensity of the probe beam is sufficient to saturate the transition, the absorbed power P is expected to be proportional to the number of atoms N, as $P = Nh\nu\Gamma/2$ in the limit of full saturation (ν is the laser frequency). This requires about 10 mW. It allows us to measure the number of atoms in the MOT, where the absorption is about 1 mW, which corresponds to 10^9 atoms. When the cloud is evaporated in the magnetic trap, the power absorbed in the probe pulse becomes weaker, so that it is difficult to measure the total absorption on the photodiode PD for low temperature clouds. To overcome this problem, a solution, which we didn't implement, would consist in making the probe beam size smaller.

Instead, the number of atoms in the evaporated clouds is deduced from the absorption images on the CCD camera. The value of the absorption cross-section ($3\lambda^2/2\pi$) is corrected down in order to take into account various effects that tend to lower it, as Doppler effect, light and atom polarization, and finite linewidth of the probe laser (see the discussion in [2]). The precision of this measurement is rather poor, but proper corrections allow a reasonable agreement (within a factor 2) between the number of atoms we extract from the image of a cloud at relatively high temperature (1 mK) with the one we measured by saturating the absorbed intensity.

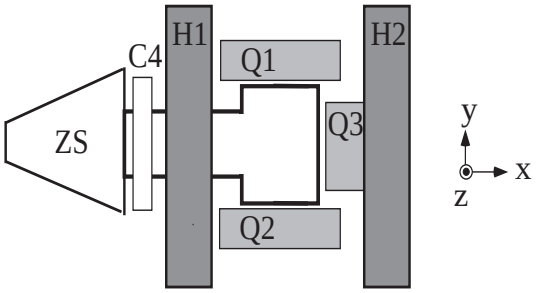

Fig. 2. Magnetostatic trap. ZS is the Zeeman slower coil, Q1, Q2 and Q3 the Ioffé-Prichard coils, H1 and H2 are the bias compensation coils. C4 is a coil used to compensate the field created by ZS at the center of the cell.

4 Loading the magnetic Ioffé-Pritchard trap

4.1 Description of the trap

The magnetostatic trap that we are using for the confinement of the cold gas is sketched in Figure 2. It is constituted by three coils Q1, Q2 and Q3 of relatively small size which realize a Ioffé-Pritchard trap. A set of two larger Helmholtz coils H1 and H2 are added in order to compensate the bias field. The third coil Q3 has 108 turns of 1 mm diameter copper wire, with an inner diameter of 2 cm. The Helmholtz coils are made of 44 turns of hollow copper tube of 5 mm diameter. Their inner diameter is about 11 cm, they produce a field of 110 G for 46.6 A, which compensates the bias field down to about 5 G. Also, we can use an additional set of Helmholtz coils wound on top of coils H1 and H2, in order to finely adjust the bias and reduce it even more for further compression of the trap. The curvature of the field is 190 G/cm^2 along x, with gradients of 265 G/cm along the radial directions, when we run 46.6 A through the three coils Q1, Q2, Q3. The trap depth is then about 16 mK. The trap frequency along x is $\nu_x = 115$ Hz. The radial frequency is $\nu_{\rm perp} = 190$ Hz without the compensation of the bias, and 985 Hz with a 5.1 G bias field.

The distance of the 3 coils from the center of the cell is 26 mm for Q1 and Q2, but 28 mm for Q3. Due to geometrical constrains, this 3 coils trap is asymmetrical. As a consequence the center of this trap is shifted by 5 mm compared to the center of the initial MOT.

4.2 Compression, molasses, optical pumping

When the loading of the MOT is over, the center of the cloud has to be shifted by about 5 mm along the x-direction in order to be at the central position of the magnetostatic trap.

This displacement is produced by the magnetic field of the Zeeman Slower (ZS in Fig. 2). During the loading of the MOT, the coil C4 (see Fig. 2) placed at the end of ZS produces a field along x fairly homogeneous at the center of the cell, where it compensates the field produced by ZS. When the loading is over, C4 is switched off whereas ZS remains on. This shifts the position of the zero of the quadrupolar field created by Q1 and Q2 towards the center of the magnetic trap. The center of the MOT is also shifted when the field gradient provided by Q1 and Q2 is decreased. We typically decrease this gradient by a factor of 2, at the same time when C4 is switched off, in order to shift the cloud by the required 5 mm. This also decompresses the MOT. During this process, which lasts for 10 ms before reaching an equilibrium, the laser beams of the MOT are left on.

The spatial shift of the cloud is followed by a compression phase, in order to increase the density before loading the magnetic trap. The field gradient being now fixed, one decreases the detuning down to 30 MHz keeping the same intensity in the MOT beams. This detuning is adjusted so that the cloud gets compressed without any sensible losses due to Penning collisions. At the end of this 6 ms compression phase, the final rms radii are about 2 mm.

We then apply an optical molasses phase, in order to decrease the temperature of the gas before the loading into the magnetic trap. The MOT magnetic field gradient is thus turned off. The laser beams are kept on with a different detuning (typically -1 MHz) and a lower intensity, these two parameters being adjusted to avoid loosing trapped atoms. The molasses pulse duration is of 0.5 ms, the equilibrium temperature being typically 300 μK, which is still large compared to the Doppler limit (40 μK). Large absorption of the laser beams might prevent the molasses to be fully efficient.

The next step is an optical pumping phase. It is used to put as many atoms as possible in the same low-field seeking magnetic substate of the 2^3S_1 state so as not to loose most of them when loaded into the magnetostatic trap, which only retains atoms in the $m_J = +1$ sublevel. The optical pumping laser field is made out of two independent beams, aligned along the x-axis, forming a standing wave, where both beams are σ_+ polarized with respect to the direction of the bias filed. The pulse that optimizes the transfer efficiency lasts 50 μs, its intensity is $I/I_{\rm sat} = 1.4$, and its frequency is detuned by -6 MHz from resonance. The efficiency of the optical pumping pulse is measured by comparing the number of atoms transferred in the magnetic trap with and without optical pumping. Using the optical pumping pulse typically multiplies this number by a factor of 2.

4.3 Mode-matching and compression

In order not to loose on the phase-space density, a proper mode matching has to be made to adapt the atomic cloud in the MOT to the potential created by the magnetic trap. The best method is to keep the same aspect ratio (1.65) and temperature (300 μK) before and after transfer. One calculates that this requires to transfer the atoms in the trap created by the three coils Q1, Q2 and Q3, using a current of only 5 A. The trap is typically switched on at a current of 5 A within about 2 ms. After 10 ms, the number of atoms that remain trapped is only one third of the initial number when the optical pumping pulse is not used,

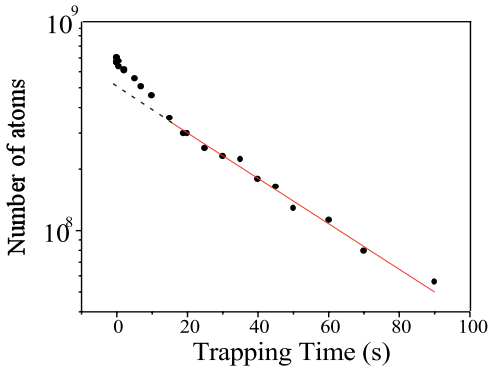

Fig. 3. Lifetime of the cloud in the magnetostatic trap at a temperature of 1.4 mK.

as expected if one assumes that atoms are initially equally distributed among the three Zeeman sublevels. Using the optical pumping pulse, we end up with 7×10^8 trapped atoms, compared to 10^9 atoms initially in the MOT.

Then, the cloud is compressed by ramping the current in these three coils to its final value of 46.6 A. This compression stage has to be adiabatic, which implies to increase the trap confinement on a time scale much longer than the oscillation period. We choose typically 1 s. The following step is to compensate the bias field by turning on the current into the coils H1 and H2: the field B_0 along x then decreases within 1 s. After the final compression stage, the same current (46.6 A) runs through all the coils of the trap. The temperature, measured by time of flight, has increased up to 1.4 mK. At this temperature, the harmonic approximation does not hold, the trap is semi-linear. The central density is calculated to be 8.4×10^{10} atoms/cm^3, using the measured temperature and number of atoms of the thermalized cloud.

4.4 Lifetime of the cloud in the magnetic trap

Once the atomic cloud has been loaded into the magnetic trap, one can measure the number of atoms as a function of time. The result of this measurement is shown in Figure 3.

The half-time is measured to be about 15 s. This rather long lifetime shows that the Penning ionization collisions between metastable helium atoms are inhibited by the spin polarization in the $m_J = +1$ sublevel, as predicted by theory [9–12] and already observed to some extent in a MOT [13], and in a magnetic trap [14]. Indeed, if the collision rate had been equal to that in the non polarized case, namely $\beta \simeq 10^{-10}$ cm^3/s [15–17,12,18], the half-time of the cloud in the magnetostatic trap would not have exceeded 1 s. This thus indicates that Penning collisions are suppressed by at least one order of magnitude.

The decay is not purely exponential yet (see Fig. 3), as expected if inelastic collisions between trapped particles are important. Assuming that the losses are due to collisions with the background gas as well as collisions between trapped metastable atoms, a fit of the decay gives a lifetime of 58 s due to background collisions, and a two-body decay rate constant $\beta = 1.1 \times 10^{-12}$ cm^3/s. We know from the success of the evaporation and the study of the losses at higher densities that the two-body loss rate constant is two order of magnitude smaller. This initial non-exponential decay thus cannot be explained by inelastic collisions. One possible explanation is that the initial loss is due to the natural evaporation of the hottest atoms. If we fit the last part of the decay curve with an exponential law (straight line in Fig. 3), we extract a lifetime due to background collisions of 40 s.

The value of the lifetime was found quite dependent on the operation conditions of the atomic source: the higher the pressure in the discharge chamber, the shorter the lifetime. This indicates that helium atoms in the ground state, not perfectly spatially filtered by the apparatus, contribute significantly to the residual vacuum. If after loading the magnetic trap one closes the UHV valve which disconnects the atomic source from the rest of the set up, the lifetime goes up to 88 s. However closing such a valve between each measurement would be very unpractical and one usually operates with lifetimes of about 40 s, corresponding to a pressure in the source chamber of 2×10^{-5} mbar. This value is long enough to ensure the success of the rest of the cooling procedure.

5 Evaporative cooling

5.1 Starting the evaporation

Before starting the evaporative cooling, it is useful to estimate the initial collisional rate, in order to determine whether the evaporative cooling can enter the so-called runaway regime, where the phase space density increases exponentially with time. This regime can be reached if the mean rate of elastic collisions $\bar{\gamma}_{\rm col}$ is much larger than the rate of inelastic collisions $\Gamma_{\rm in}$. A good criteria is $r = \bar{\gamma}_{\rm col}/\Gamma_{\rm in} > r_{\rm c} = 34$ for a semi-linear trap [19].

In order to estimate $\bar{\gamma}_{\rm col}$, we measure the time τ it takes for a cloud initially out of equilibrium to return to thermal equilibrium in the trap. This thermalization time is inversely proportional to the collisional rate: one can show with a Monte-Carlo numerical simulation that $\tau = 2.7/\bar{\gamma}_{\rm col}$ [20,21].

To prepare the cloud out of equilibrium, we compress the trap by lowering the bias field within 20 ms. This is too short to obtain thermal equilibrium, but slow enough to ensure adiabatic compression in the transverse directions. At the end of the compression, the temperatures along the transverse and longitudinal directions are different. One can then monitor the evolution of the ellipticity during the thermalization, which relaxes to its equilibrium value in the trap. After a variable delay, the trap is switched off and we measure the size of the cloud after a 0.5 ms expansion time. The evolution of the ellipticity of the cloud is shown in Figure 4.

We fit the ellipticity by an exponential law, which gives a thermalization time $\tau = 92$ ms. The mean collisional rate is thus about 30 s^{-1}, at a temperature of 1.4 mK. As this measurement was performed with 5×10^8 atoms, one can estimate the elastic rate constant $\alpha = \langle \sigma v \rangle =$

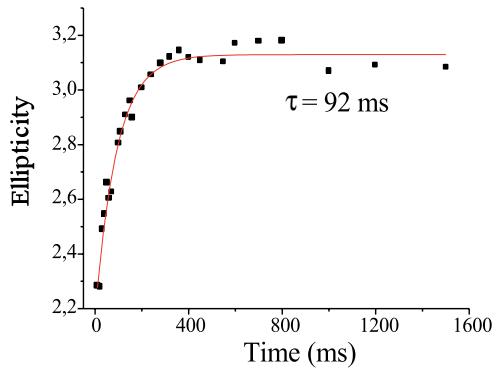

Fig. 4. Thermalization of the cloud after loading the magnetostatic trap. The ellipticity of the cloud relaxes with a time constant of 92 ms to its value at thermal equilibrium. The final temperature is 1.4 mK.

$\bar{\gamma}_{\rm col}/\bar{n}$, where $\bar{n}$ is the average density, σ the scattering cross-section, v the relative velocity, and $\langle\ \rangle$ denotes the average over the thermal distribution. With $\bar{n} = 1.1 \times 10^{10}$ cm^{-3}, one finds $\alpha = 2.8 \times 10^{-9}$ cm^3/s, which agrees reasonably well with the measurement performed in [22]: $\alpha = 5 \times 10^{-9}$ cm^3/s to within a factor of 3 at 1 mK, and with the theoretical prediction of [10], where $\alpha \simeq 4 \times 10^{-9}$ cm^3/s. As the lifetime was measured to be 40 s, this gives a ratio $r = 1200$, which exceeds $r_{\rm c}$ by far: the evaporation should thus be fast.

5.2 Optimization of the ramp

Evaporative cooling is performed by inducing RF spin-flips with an auxiliary coil placed on top of the quartz cell, 3 cm away from the cloud. This 3-turns coil is connected to a radio-frequency synthetizer and a 10 W RF amplifier. The radio-frequency of the evaporation is lowered in a piecewise linear fashion in 6 steps.

We adjust the duration and RF power of each segment in order to increase the collisional rate, but minimizing the loss of atoms, according to the following procedure. We first set the initial and final frequencies of each segment. The collisional rate is then measured for each segment as a function of its duration. At the beginning, it increases with time, and then reaches a plateau. We terminate each segment as soon as the plateau is reached.

The evaporation ramp starts at a frequency of 200 MHz and lasts for about 8 s. Figure 5 shows the temperature (measured by time of flight on the CCD camera at the end of each segment of the evaporation ramp) as a function of time. The parameter η, defined as the ratio between the cut-off energy and the thermal energy $k_{\rm B}T$, remains larger than 6 during all the evaporation cooling.

Figure 6 shows the increase in phase space density as well as the decrease in number of atoms during the evaporation ramp. This cooling process is very efficient as the phase space density increases by 6 orders of magnitude, while only two orders of magnitude are lost on the number of atoms.

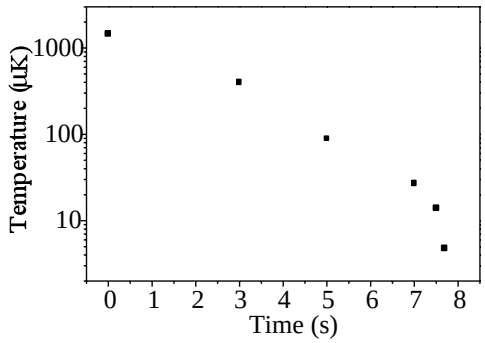

Fig. 5. Temperature during the evaporative cooling ramp. The temperature is measured by time of flight after each segment of the evaporation ramp.

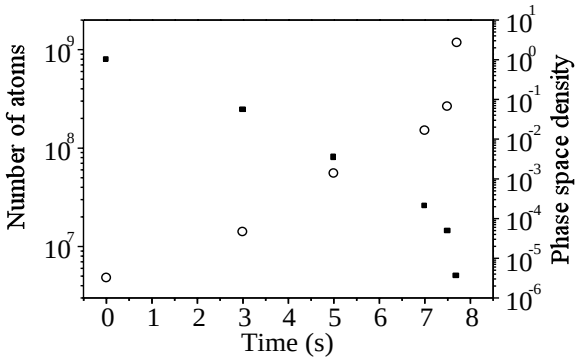

Fig. 6. Evolution of the number of atoms (squares) and the phase-space density (open circles) during the evaporative cooling.

6 Bose-Einstein condensation

When the final frequency of evaporation falls below about 14.5 MHz, one crosses the BEC transition. As compared to the results first reported in [2], the duration of the ramp is shortened. The final frequency is also slightly higher: this comes from a small difference in the bias field, which we attribute to thermal effects, as the shortening of experimental sequence results in a different temperature of the trap coils.

On the time of flight pictures taken with the CCD camera, we observe a double structure in the density profile of the cloud, corresponding to a Bose-Einstein condensate and a non-condensed cloud (see Fig. 7). The pictures are fitted by the sum of a g_2 function, valid for the thermal cloud close to the transition, and an integrated paraboloidal distribution, that describes the density profile of the condensate in the Thomas-Fermi limit. From the pictures, we can extract the condensed fraction as a function of the normalized temperature ($T_{\rm c}(N) = (N/1.202)^{1/3}\hbar\bar{\omega}/k_{\rm B}$), which we show in Figure 8. We measure a critical temperature $T_{\rm c} = 4.7 \pm 0.5$ μK.

A proper calibration of the number of atoms at the transition is difficult if we extract this number from the absorption images, as already discussed in [2]. The number of atoms at the transition is thus inferred from the critical temperature, using $N_{\rm c} = 1.202(k_{\rm B}T_{\rm c}/\hbar\bar{\omega})^3$, where $\bar{\omega}$ is

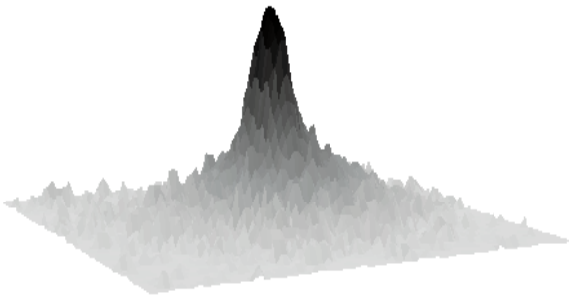

Fig. 7. Three-dimensional absorption image of the cloud after the BEC transition has been crossed.

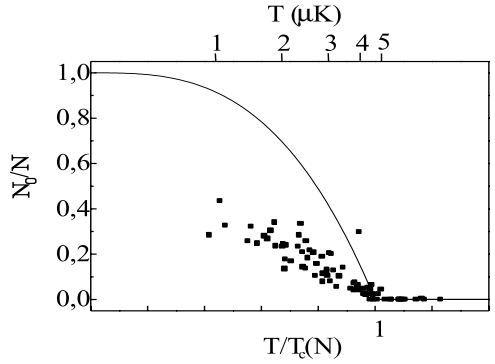

Fig. 8. Condensed fraction as a function of the reduced temperature, as well as the temperature. N_0 is the number of atoms in the condensate, and N the total number of atoms. The squares are the experimental data, whereas the line is the prediction for a non-interacting gas.

the geometrical average of the frequencies of the trap. As a consequence, the normalized temperature in Figure 8 is 1 at the transition. The experimental points deviate strongly from the theoretical curve for the non-interacting cloud, which could be explained by mean-field effects.

The formula used to estimate N_c is in principle valid only for a perfect gas. The critical temperature is also expected to be slightly shifted by the interactions [23,24]. As the effect of the interactions in an harmonic trap is still a debated issue [25], we choose this value of N_c to estimate the scattering length a, because it is easier to trace down the error on N_c when derived from T_c. We deduce $N_c = 8.2\times10^6$ atoms with an uncertainty of about 30%, whereas the absorption image of a cloud at the threshold on the CCD camera gives $N_c = 5 \times 10^6$.

This allows us to calibrate the absorption images of the cloud in the region 5 to 1 μK, and extract the number of atoms in the condensate by comparison with the number at the transition (see Fig. 9).

The number of atoms in the condensate is at most $N_0 = 6 \times 10^5$, and is roughly constant in the range from 1 to 3 μK. We believe this number does not increase when the temperature is decreased below the critical temperature because of strong losses, which might be due to inelastic collisions and secondary processes.

Finally, we can give an estimate of the scattering length a using $a = (\sigma/15N_0)(2\mu/\hbar\bar{\omega})^{5/2}$, where $\sigma = (\hbar/m\bar{\omega})^{1/2}$ is the characteristic size of the ground state of the trap, and μ is the chemical potential. Within the Thomas-Fermi approximation, μ can be deduced from the measurement of the size of the condensate [26], $\mu = 1.4 \times 10^{-29}$ J. We finally find $a = 16 \pm 8$ nm, which is consistent with theoretical calculations, as well as with the measurement of [1], which gives $a = 20 \pm 10$ nm.

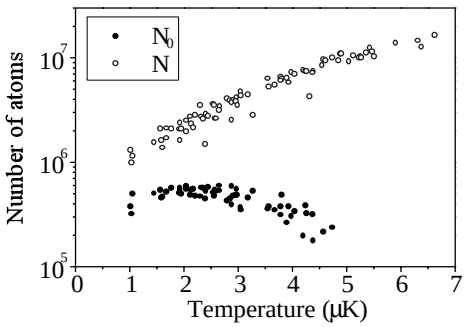

Fig. 9. Number of atoms N_0 in the condensate, and total number of atoms N, as a function of the temperature.

The typical lifetime of the number of atoms in the condensate is about 2 s. This is significantly lower than the lifetime due to background collisions, indicating that losses are due to inelastic collisions between atoms in the condensate. In the present stage of the experiment, it is not possible to discriminate between 2-body or 3-body decay. If one assumes now that 3-body collisions between atoms in the condensate are responsible for the decay of N_0 [27], one can give an upper bound for the rate constant L defined by $\dot{N}(t) = -L\int n^3(\mathbf{r})\mathrm{d}^3r$. Fitting our data gives $L \leq (2.8 \pm 0.2) \times 10^{-27}$ cm^6/s. This value can be compared to theoretical predictions [28,29]: for example, our upper limit is compatible with [28], which finds $L = 3.9\hbar a^4/2m = 2 \times 10^{-27}$ cm^6/s. A more precise measurement would require to improve the stability of the experiment in order to decrease the statistical errors, and include the presence of the atoms remaining in the thermal cloud in the analysis of the condensate decay.

7 Conclusion

We conclude that the procedure for BEC of a metastable helium gas is now well mastered. The final step of evaporative cooling is a fast and efficient process. There are several key points to pay attention to. The most important is by far the achievement of a large enough initial density before starting the evaporation, because this is the condition for a fast enough process as compared to the intrinsic lifetime of the cloud. This implies that great care be given to the efficient loading of the MOT. Finally the quality of the vacuum is also very important, even if improving it below a certain level brings no further benefit to the experiment.

One can wonder what sort of improvements could lead to a better condensate with more atoms. A different geometry for the MOT beams could prevent losses during the slowing of the atomic beam (see [7] for more details),

and increase the number of atoms in the MOT. It is also possible to reduce further the bias field down to a fraction of a gauss, and optimize the evaporative cooling in a tighter trap. This would increase the density and the elastic collision rates, but also the inelastic collision rates and heating processes, so that it is not obvious that more compression would result in more atoms in the BEC.

The detection is purely optical, which has the advantage of allowing the measurement of the size of the atomic cloud. Yet, the effect of the probe pulse and the present difficulties of calibration of the number of atoms have to be better understood. A detection set-up using visible light could simplify the detection scheme, as CCD cameras have a much better efficiency in the visible. Of course a crucial improvement will be to introduce a channelplate as in [1]. An ideal experiment would combine both the optical and the channelplate detection systems.

This work was supported by La Région Ile-de-France through SESAME contract number 521027.

References

1. A. Robert, O. Sirjean, A. Browaeys, J. Poupard, S. Nowak, D. Boiron, C.I. Westbrook, A. Aspect, Sci. Mag. **292**, 463 (2001).
2. F. Pereira Dos Santos, J. Léonard, Junmin Wang, C.J. Barrelet, F. Perales, E. Rasel, C.S. Unnikrishnan, M. Leduc, C. Cohen-Tannoudji, Phys. Rev. Lett. **86**, 3459 (2001).
3. M.H. Anderson, J. Ensher, M. Matthews, C. Wieman, E. Cornell, Sci. Mag. **269**, 198 (1995).
4. K.B. Davis, M.O. Mewes, N. van Druten, D. Durfee, D. Kurn, W. Ketterle, Phys. Rev. Lett. **75**, 3969 (1995).
5. C.C. Bradley, C.A. Sackett, J.J. Tollett, R.G. Hulet, Phys. Rev. Lett. **75**, 1687 (1995); see also C.C. Bradley, C.A. Sackett, R.G. Hulet, Phys. Rev. Lett. **78**, 985 (1997).
6. D. Fried, T. Killian, L. Willmann, D. Landhuis, S. Moss, D. Kleppner, T. Greytak, Phys. Rev. Lett. **81**, 3811 (1998).
7. F. Pereira Dos Santos, F. Perales, J. Léonard, A. Sinatra, Junmin Wang, F.S. Pavone, E. Rasel, C.S. Unnikrishnan, M. Leduc, Eur. Phys. J. AP **14**, 69 (2001).
8. F. Pereira Dos Santos, F. Perales, J. Léonard, A. Sinatra, Junmin Wang, F.S. Pavone, E. Rasel, C.S. Unnikrishnan, M. Leduc, Eur. Phys. J. D **14**, 15 (2001).
9. G.V. Shlyapnikov, J.T.M. Walraven, U.M. Rahmanov, M.W. Reynolds, Phys. Rev. Lett. **73**, 3247 (1994).
10. P.O. Fedichev, M.W. Reynolds, U.M. Rahmanov, G.V. Shlyapnikov, Phys. Rev. A **53**, 1447 (1996).
11. V. Venturi, I.B. Whittingham, P.J. Leo, G. Peach, Phys. Rev. A **60**, 4635 (1999).
12. V. Venturi, I.B. Whittingham, Phys. Rev. A **61**, 060703-1 (2000).
13. N. Herschbach, P.J.J. Tol, W. Hogervorst, W. Vassen, Phys. Rev. A **61**, 050702(R) (2000).
14. S. Nowak, A. Browaeys, A. Robert, D. Boiron, C.I. Westbrook, A. Aspect, Appl. Phys. B **70**, 455 (2000).
15. H.C. Mastwijk, J.W. Thomsen, P. van der Straten, A. Niehaus, Phys. Rev. Lett. **80**, 5516 (1998).
16. M. Kumakura, N. Morita, Phys. Rev. Lett. **82**, 2848 (1999).
17. P.J.J. Tol, N. Herschbach, E.A. Hessels, W. Hogervorst, W. Vassen, Phys. Rev. A **60**, R761 (1999).
18. P.J. Leo, V. Venturi, I.B. Whittingham, J.F. Babb, Phys. Rev. A **64**, 042710 (2001).
19. J. Walraven, in "Quantum Dynamics of Simple Systems", Vol. 44 of *Scottish Universities Summer Schools in Physics Proceedings*, edited by G.-L. Oppo, S. Barnett, E. Riis, W. Wilinson (Institute of Physics, Bristol, 1996), p. 315.
20. C.R. Monroe, E.A. Cornell, C.A. Sackett, C.J. Myatt, C.E. Wieman, Phys. Rev. Lett. **70**, 414 (1993).
21. H. Wu, C. Foot, J. Phys. B **29**, L321 (1996).
22. A. Browaeys, A. Robert, O. Sirjean, J. Poupard, S. Nowak, D. Boiron, C.I. Westbrook, A. Aspect, Phys. Rev. A **64**, 034703-1 (2001).
23. S. Giorgini, L.P. Pitaevskii, S. Stringari, Phys. Rev. A **54**, R4633 (1996).
24. G. Baym, J.-P. Blaizot, M. Holzmann, F. Laloë, D. Vautherin, Phys. Rev. Lett. **83**, 1703 (1999).
25. Effects due to mean field have been calculated for an harmonic trap [23] and effects due to quantum correlations have been calculated in a box [24]. The shift of the critical temperature T_c can be quite large ($\delta T_c/T_c \simeq 15\%$) for both of these effects, due to the large value of the scattering length a, but they have opposite signs. It would be interesting to study them both in more detail for an harmonic trap.
26. See for example, F. Dalfovo, S. Giorgini, L.P. Pitaevskii, S. Stringari, Rev. Mod. Phys. **71**, 463 (1999).
27. A. Aspect, private communication.
28. P.O. Fedichev, M.W. Reynolds, G.V. Shlyapnikov, Phys. Rev. Lett. **77**, 2921 (1996).
29. B.P. Esry, C.H. Greene, J.P. Burke, Phys. Rev. Lett. **83**, 1751 (1999).